Adaptive Beamforming Applied to Coherent MIMO Radar-over-Fiber Systems

Salvatore Maresca
IEIIT Institute
National Research Council (CNR)
Pisa, Italy
salvatore.maresca@cnr.it

Malik Muhammad Haris Amir
TeCIP Institute
Sant'Anna School of Advanced Studies (SSSA)
Pisa, Italy
malikmuhammadharis.amir@santannapisa.it

Filippo Scotti
PNTLab Institute
Nat. Interuniv. Cons. for Telecom. (CNIT)
Pisa, Italy
filippo.scotti@cnit.it

Mirco Scaffardi
PNTLab Institute
CNIT
Pisa, Italy
mirco.scaffardi@cnit.it

Paolo Ghelfi
PNTLab Institute
CNIT
Pisa, Italy
paolo.ghelfi@cnit.it

Antonella Bogoni
PNTLab Institute
CNIT
Pisa, Italy
antonella.bogoni@cnit.it

Antonio Malacarne
PNTLab Institute
CNIT
Pisa, Italy
antonio.malacarne@cnit.it

2024 IEEE Radar Conference (RadarConf24) | 979-8-3503-2920-9/24/$31.00 ©2024 IEEE | DOI: 10.1109/RADARCONF2458775.2024.10549749

***Abstract*—In this paper, adaptive beamforming (ABF) techniques are applied to a coherent multiple-input multiple-output (MIMO) radar-over-fiber (RaoF) network for precise target localization. In the proposed system, a common central unit transmits and receives radio-frequency signals through optical standard single-mode fiber (SSMF) links, to/from remoted radar transmitters and receivers placed along a linear baseline. Electro-optical conversion is achieved through direct modulation of low-cost, power-effective, and high-speed vertical-cavity surface-emitting lasers (VCSELs).**

Among the available MIMO-ABF techniques, both data-independent and data-dependent approaches are taken into account. In particular, one estimation technique per family is analyzed (i.e., data-independent, data-dependent without array steering vector errors and data-dependent with array steering vector errors), i.e., respectively the least-squares estimator, the Capon and the robust Capon beamforming techniques.

The advantages and disadvantages of these techniques are illustrated through their application to experimental X-band data acquired with a MIMO RaoF system in a controlled scenario.

***Index Terms*—Microwave Photonics, MIMO Radar, Radio-over-Fiber, Radar-over-Fiber, Signal Coherence, Adaptive Beamforming, Least-Squares, Capon Beamformer, Robust Capon Beamformer.**

I. Introduction

Today, radar systems, thanks to the ever increasing miniaturization of electronic components, have rapidly become pervasive in high-precision civilian and industrial applications, such as road traffic monitoring, collision avoidance systems, control of industrial assembly lines and conveyors, as well as body-scan imaging for medicine and security [1], [2].

The project leading to this pubblication has received funding from Frontex under the Frontex Research Grants Programme. Call for Proposals 2022/CFP/RIU/01 - Grant Agreement No. 2023/350. This pubblication reflects only the authors' view. Neither the European Union nor Frontex are responsible for any use that may be made of the information it contains.

This work has also been partially funded by the EU under the Italian National Recovery and Resilience Plan (PNRR) of NextGenerationEU partnership on "Telecommunications of the Future" (PE00000001 - program "RESTART").

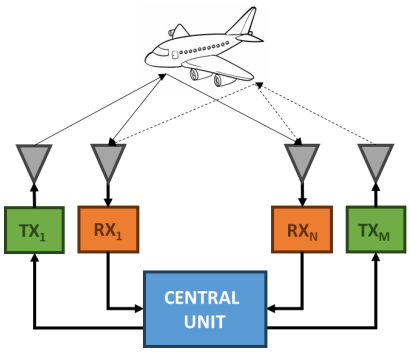

Fig. 1. MIMO radar with widely separated antennas formed by one central unit (CU), acting as the fusion centre, and M transmit (TX) and N receive (RX) remote antennas.

Thus, the ever increasing demand of systems with superior resolution, stability and accuracy in the monitored area, is pushing radars to become even more ubiquitous sensors [3].

The development of the multistatic radar concept presented in [4], following a more *network-oriented* approach, led to the theorization, almost twenty years ago, of the idea of multiple-input multiple-output (MIMO) radars [5].

These can be distinguished between systems with co-located antennas [6] and systems with widely separated antennas [7]. This second type employs multiple, spatially distributed transmitters (TXs) and receivers (RXs) that can be driven by one central unit (CU). In particular, multiple sparse radars grant improved target detection performance by exploiting radar cross section (RCS) diversity [8], improved detection of slow-moving targets [9], and high-resolution target localization [10].

In the centralized architecture in Fig. 1, the CU provides the TX front-ends with the signals to be transmitted. In reception, the signals received by the RX front-ends are routed back to the CU, where they are jointly processed in a coherent manner.

This architecture allows a better exploitation of the infor-

mation content carried by the signals for target detection and imaging. However, long-term frequency and phase coherence among the signals to/from the radar front-ends is required.

In this context, microwave photonics (MWP) has emerged as a possible enabling technology for implementing coherent MIMO radars with widely separated antennas [11]–[14].

In this paper, following the work presented in [15], a coherent MIMO radar-over-fiber (RaoF) network is presented, where a common CU transmits and receives radio frequency (RF) signals through optical standard single-mode fiber (SSMF) links, to/from two remote TX and four RX radar front-ends, distributed along a 3 m baseline. The distinctive feature of this solution is that electro-optic conversion is achieved through direct modulation (DM) of low-cost, power-effective, and high-speed vertical-cavity surface-emitting lasers (VCSELs) working in the 1.3μm wavelength range.

The system is tested in a down-scaled scenario, using an RF carrier of 8.5 GHz, due to the limited modulation bandwidth of the employed VCSELs. However, potential VCSEL modulation bandwidth can be > 30 GHz [16].

System performance is evaluated considering 1 GHz bandwidth signals, and comparing non-coherent and coherent MIMO signal processing outputs. This latter elaboration confirms the potential of a coherent system to achieve superior resolution than non-coherent data fusion.

In addition, stepping from the analysis presented in [17], which was conceived for MIMO radars with co-located antennas, this paper investigates the possibility to apply adaptive beamforming (ABF) techniques also to systems employing widely separated antennas. Moreover, this work pushes forward the research activities in [18], in which the ABF techniques were applied to simulated study cases, under both ideal and non-ideal conditions. In this paper, the experimental aim is to demonstrate, with a real coherent MIMO radar, the improvement in target localization and sidelobe suppression capabilities with respect to standard MIMO processing.

The remainder of the paper is organized as follows. In Section II, MWP techniques for MIMO radars are described. In Section III, both standard and ABF processing techniques for MIMO radars are presented. The experimental setup is described in Section IV, whereas the analysis of results is reported in Section V. Conclusions and perspectives are given in Section VI.

II. Microwave Photonics for MIMO Radars

The potential benefits brought by MWP techniques can be illustrated by referring to the MIMO radar network concept scheme depicted in Fig. 2, see also [14]. In the most general sense, the CU includes a laser source, whose task is to enable the distribution of the electrical signals through the optical domain. Depending on system requirements in terms of complexity and cost, two types of lasers can be used: *i)* single-frequency, or *ii)* multi-frequency lasers.

A. Systems implementing single-frequency lasers

Here, the use of photonics is limited to the distribution of the signals, conventionally generated and received at RF, through

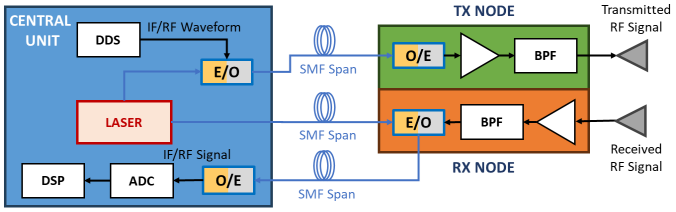

Fig. 2. High-level MIMO radar system architecture. ADC: analog-to-digital converter; BPS: band-pass filter; DDS: direct digital synthesizer; DSP: digital signal processing; O/E: opto-electronic; IF: intermediate frequency; E/O: electro-optical; RF: radio-frequency; RP: radar peripheral; RX: receiver; SMF: single-mode fiber; TX: transmitter.

cheap high-capacity optical links. The signal is digitally synthesized at RF by the electrical direct digital synthesizer (DDS). Electro-optic (E/O) conversion is achieved through DM of the laser source (e.g., a VCSEL).

This solution, as in radio-over-fiber (RoF) systems, is ideal for applications requiring massive low-cost production, power efficiency, as well as system compactness, as in advanced driver-assistance systems. Moreover, this solution permits to avoid electro-magnetic interference (EMI), minimize the optical loss and signal distortion with respect to an RF-only system, at the same time maintaining the coherence among the distributed signals.

B. Systems implementing multi-frequency lasers

Even in this type of architecture, signals are distributed through optical links but the signal is synthesized at intermediate frequency (IF). Through E/O modulation, the IF signal is transferred onto an optical frequency comb, e.g., a mode-locked laser (MLL). Consequent RF up-conversion is then achieved at a remote node through O/E conversion, i.e., photodetection. Similarly, at each node E/O conversion driven by RF echo signals and followed by photodetection at the CU, implements the signal down-conversion.

This way the CU can manage multiple distributed radar TX and RX nodes, granting excellent phase stability in multi-band signal generation and reception, as well as preserving phase stability upon signal distribution through fiber links [14].

III. Adaptive Beamforming for MIMO Radar

A. Signal Model

The received signal matrix can be written as in [17]:

$$\mathbf{X} = \mathbf{a}_{RX}(\theta)\,\beta(\theta)\,\mathbf{a}_{TX}^{t}(\theta)\,\mathbf{S} + \mathbf{Z}, \tag{1}$$

where:

- $\mathbf{X} \in \mathbb{C}^{N\times L}$: RX signal matrix;
- M/N: arbitrarily located TX/RX antennas;
- L: number of samples;
- $\mathbf{a}_{RX}(\theta) \in \mathbb{C}^{N\times 1}$: RX antenna steering vector;
- $\mathbf{a}_{TX}(\theta) \in \mathbb{C}^{M\times 1}$: TX antenna steering vector;
- $\mathbf{S} = [\mathbf{s}_1, \ldots, \mathbf{s}_M]^t$: TX signal matrix;
- $\mathbf{s}_m \in \mathbb{C}^{L\times 1}$: generic TX signal at the m-th antenna element, with $m = 1, 2, \ldots, M$;

- $\beta(\theta) \in \mathbb{C}^{1\times 1}$: complex amplitude of the reflected signal from θ, proportional to the RCS of the focal point θ;
- $\mathbf{Z} \in \mathbb{C}^{N\times L}$: residual noise term (e.g., un-modeled noise, interference from targets, jamming).

For conciseness, in the following of this paper the dependency of $\mathbf{a}_{RX}(\theta)$ and $\mathbf{a}_{TX}(\theta)$ from θ will be omitted.

B. MIMO Standard Processing

Typical monitoring applications, such as coastal surveillance and air traffic control, often require that a radar system is able to switch among different operating modes (e.g., detection, tracking, imaging), adapting the resolution and, thus, the computational complexity to the specific operative situation.

Similarly, MIMO radars with widely separated antennas can employ two operating modes: *i)* a standard *search mode* for target detection with low resolution demands, and *ii)* an *imaging mode* with more stringent resolution constraints. The former type of processing is based on non-coherent processing, whereas the latter requires coherent processing, to obtain resolution beyond the one granted by the waveform bandwidth.

For brevity the mathematical discussion of these two methods is omitted. Information can be found in [7].

C. Adaptive Beamforming Techniques

In MIMO radars with co-located antennas, by transmitting independent waveforms through different antennas, the echoes due to targets at different locations result linearly independent each other. As stated in [17], this condition may allow the direct application of ABF techniques. This is even more evident in MIMO radars with widely separated antennas, which also exploit geometric diversity.

MIMO-ABF techniques can be divided into data-independent and data-dependent approaches. The least squares (LS) method belongs to the first category [17]. Instead, data-dependent ABF techniques can be further categorized based on their capability to deal, or not, with array steering vector errors [17]. The Capon [19], the amplitude and phase estimation (APES) [20], the combined Capon and APES (CAPES) [21] and the combined Capon and approximate maximum likelihood (CAML) [22] algorithms work well in absence of array steering vector errors. On the contrary, the robust Capon beamformer (RCB) [23], [24], and the doubly constrained robust Capon beamformer (DCRCB) [25] are more robust in presence of array steering vector errors. In this work, the LS, the Capon and the RCB estimators are considered [17].

1) LS Estimator: A simple way to estimate $\beta(\theta)$ in eq. 1 consists of using the LS method [17]:

$$\hat{\beta}_{LS}(\theta) = \frac{\mathbf{a}_{RX}^H \mathbf{X}\mathbf{S}^H \mathbf{a}_{TX}^*}{L\|\mathbf{a}_{RX}\|^2 \left[\mathbf{a}_{RX}^t \hat{\mathbf{R}}_{\mathbf{SS}} \mathbf{a}_{TX}^*\right]}, \tag{2}$$

with $\hat{\mathbf{R}}_{\mathbf{SS}} = \mathbf{S}\mathbf{S}^H/L$ and where $(.)^H$, $(.)^*$ and $(.)^t$ denote the conjugate transpose, the complex conjugate and the transpose, respectively. The operator $\|.\|$ denotes the Euclidean norm, and $\hat{\mathbf{R}}_{\mathbf{SS}}$ is the correlation matrix of the waveforms. However, being a data-independent beamforming-type method, the LS method suffers from high sidelobes and low resolution.

2) Capon Estimator: The Capon estimator is a data-dependent approach, consisting of two main steps. The first is the Capon beamforming step [19]. The second is an LS estimation step, which involves a matched filtering procedure. The Capon estimate of $\beta(\theta)$ is given as follows:

$$\hat{\beta}_{Capon}(\theta) = \frac{\mathbf{a}_{RX}^H \hat{\mathbf{R}}^{-1} \mathbf{X}\mathbf{S}^H \mathbf{a}_{TX}^*}{L\left[\mathbf{a}_{RX}^H \hat{\mathbf{R}}^{-1} \mathbf{a}_{RX}\right]\left[\mathbf{a}_{TX}^t \hat{\mathbf{R}}_{SS} \mathbf{a}_{TX}^*\right]}, \tag{3}$$

where $\hat{\mathbf{R}} = \mathbf{X}\mathbf{X}^H/L$ is the sample covariance of the observed data samples.

3) RCB Estimator: The previous methods assume that the transmitting and receiving arrays are perfectly calibrated, i.e., $\mathbf{a}_{TX}$ and $\mathbf{a}_{RX}$ are accurately known as functions of θ. The RCB estimator can be successfully applied to a MIMO radar system that suffers from calibration errors [23].

In fact, the RCB algorithm allows $\mathbf{a}_{RX}$ to lie in an uncertainty set. Without loss of generality, we assume that $\mathbf{a}_{RX}$ belongs to the uncertainty sphere $\|\mathbf{a}_{RX} - \bar{\mathbf{a}}_{RX}\|^2 \leq \epsilon$, with both $\bar{\mathbf{a}}_{RX}$, i.e., the nominal receiving array steering vector, and ϵ being given [18]. It is worth noticing that the calibration errors in $\mathbf{a}_{TX}$ will also degrade the accuracy of the estimate of $\beta(\theta)$. However, the LS approach of the Capon beamformer, see eq. 2, is quite robust against calibration errors in $\mathbf{a}_{TX}$. By using the Lagrange multiplier methodology, as described in [23], it is possible to write:

$$\hat{\mathbf{a}}_{RX}(\theta) = \bar{\mathbf{a}}_{RX}(\theta) - \left[\mathbf{I} - \lambda(\theta)\hat{\mathbf{R}}\right]^{-1} \bar{\mathbf{a}}_{RX}(\theta), \tag{4}$$

where $\mathbf{I}$ denotes the identity matrix. The Lagrange multiplier $\lambda(\theta)$ is obtained as the solution to the constraint equation [23]:

$$\left\| \left[\mathbf{I} - \lambda(\theta)\hat{\mathbf{R}}\right]^{-1} \bar{\mathbf{a}}_{RX}(\theta) \right\|^2 = \epsilon, \tag{5}$$

Once the Lagrange multiplier $\lambda(\theta)$ has been determined, $\hat{\mathbf{a}}_{RX}(\theta)$ is obtained from eq. 4. To eliminate a scaling ambiguity discussed in [23], it is necessary to scale $\hat{\mathbf{a}}_{RX}(\theta)$ such that $\|\hat{\mathbf{a}}_{RX}(\theta)\|^2 = N$. Replacing $\mathbf{a}_{RX}$ in eq. 3 with $\hat{\mathbf{a}}_{RX}$ yields the RCB estimate of $\beta(\theta)$.

IV. Experimental Setup

A. MIMO Radar-over-Fiber System

A controlled experimental setup has been implemented to replicate the operational capabilities of the MIMO RaoF system presented in [15] and to assess the performance of the MIMO-ABF techniques presented in Section III.

The system, depicted in Fig. 3, consists of a CU which delivers the RF signals to two TXs and collects the RF echo signals from four RXs. Both TX and RX front-ends are remoted with respect to the CU and distributed on a linear 3 m long baseline, through SSMF spools of about 10 m length. The TX radar front-ends employ Vivaldi-shaped wideband horn antennas with a maximum gain of about 12 dBi, whereas cheap patch antennas, with an almost constant gain of about 6 dBi in the $6-11$ GHz, are used at the RX front-ends. In such a configuration, the 2×4 VCSEL-based MIMO RaoF system, depicted in Fig. 4, employs eight separate virtual channels.

Electro-optic conversion is achieved through direct modulation of VCSELs working in the 1.3 μm wavelength range. Such an operative wavelength ensures the propagation over SSMF with negligible distortions up to the km range [15].

The system is tested in a controlled scenario and an RF carrier of 8.5 GHz is used. The choice of the maximum carrier frequency is limited by the 3 dB frequency response of the employed VCSELs.

In transmission, E/O conversion of the generated and received RF signals is achieved through the use of VCSELs, whereas in reception O/E conversion takes place through 10 GHz photo-diodes (PDs). Two channels of a Fujitsu digital-to-analog converter (DAC) with sampling rate equal to 60 GS/sec are used to generate repetitive 273 ns long linearly frequency-modulated continuous-wave (LFM-CW) signals with 1 GHz bandwidth. The two TXs transmit up- and down-sweep waveforms, with the two signals also separated in the time domain.

The number of RX front-ends is limited to four because of the maximum number of channels available on the employed real-time oscilloscope acting as ADC (i.e., Teledyne LeCroy SDA−813Zi−A, with 40 GS/s sampling rate on each of the four channels and 13 GHz analog bandwidth). A third DAC channel is used to trigger the ADC (i.e., the oscilloscope) and both DAC and ADC are referenced with a common 10 MHz tone. The CU, depicted in Fig. 3, includes E/O conversion of the LFM-CW signals through direct modulation of two VCSELs, and acquisition of the four RXs outputs through ADC, after photodetection and low-noise amplification (LNA).

The target, an aluminium soda can, is placed at $[0.22, 5.97]$ m, at the same height of the MIMO baseline (i.e., about 1 m). Channel delays are compensated for correcting the not perfect knowledge of the antenna element positions. For conciseness, the description of the digital signal processing (DSP) steps is omitted, see [15] for further information.

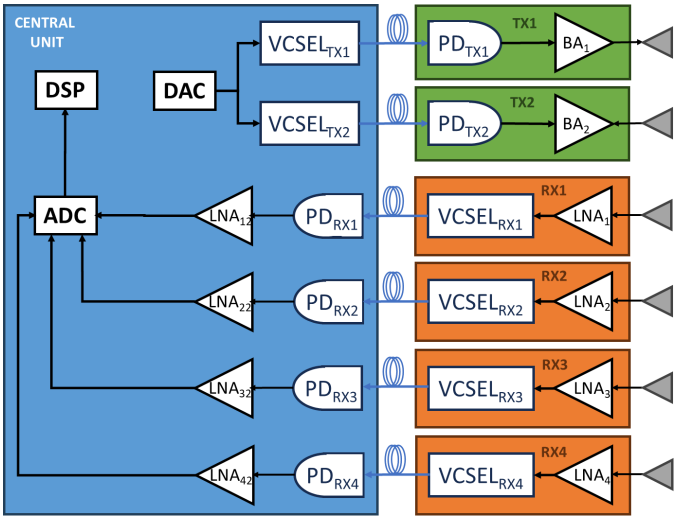

Fig. 3. Experimental setup of a 2×4 VCSEL-based MIMO RaoF system.

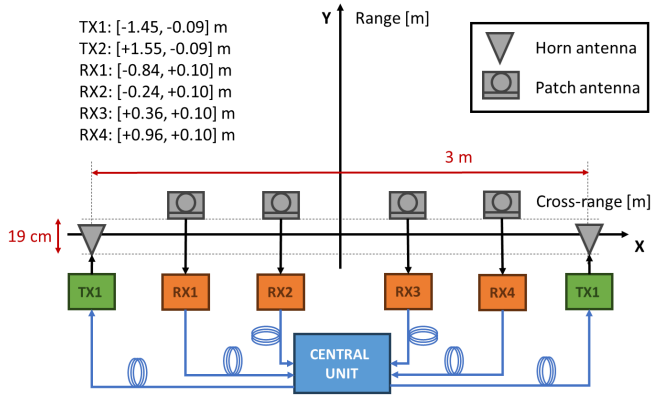

Fig. 4. Disposition of antennas along the linear baseline for the VCSEL-based MIMO RaoF system operated during the demonstration.

V. Experimental Results

In this section, standard MIMO (i.e., non-coherent and coherent), as well as MIMO-ABF techniques are applied to the data acquired by the VCSEL-based MIMO RaoF system described in Section IV.

A. Standard MIMO Processing

1) Results with simulated data: First, the experimental setup is simulated considering a single point-like target placed at the same position of the real target. Simulation results are shown in Fig. 5, where the true target position is represented by the red cross.

As described in [7], non-coherent MIMO processing consists in the super-position in the 2D space of the range profile amplitudes provided by all the MIMO virtual channels. This processing methodology allows to correctly detect the target, see Fig. 5(a). However, the target is localized with poor cross-range (i.e., angular) precision, as demonstrated by the broad horizontal extent of the uncertainty ellipsoid (i.e., the yellow banana shape) around the true target position.

Instead, by exploiting also the phase information of the range profiles and by compensating for the propagation delays, coherent MIMO processing grants improved angular resolution, which now depends on the baseline length and carrier frequency. These features allow to precisely localize the target, see Fig. 5(b). However, due to the sparseness of the antenna elements along the MIMO array baseline, harmful sidelobes, as well as azimuth ambiguities, appear in the final 2D map.

It is worth noticing that the optimization of the MIMO array configuration is out of the scope of this paper. This open problem is currently the object of ongoing investigations [26].

2) Results with real data: Results of standard MIMO processing applied to real data are shown in Fig. 6. In Fig. 6(a), the output of non-coherent MIMO processing applied to real data still provides an uncertainty ellipsoid centered at the true target position, like the one shown in Fig. 5(a). Moreover, a second uncertainty ellipsoid having lower amplitude appears at around 60 cm distance along range from the first one. Since the ground floor in the experimental setup was made by flat asphalt, the second ellipsoid could be due to the multipath

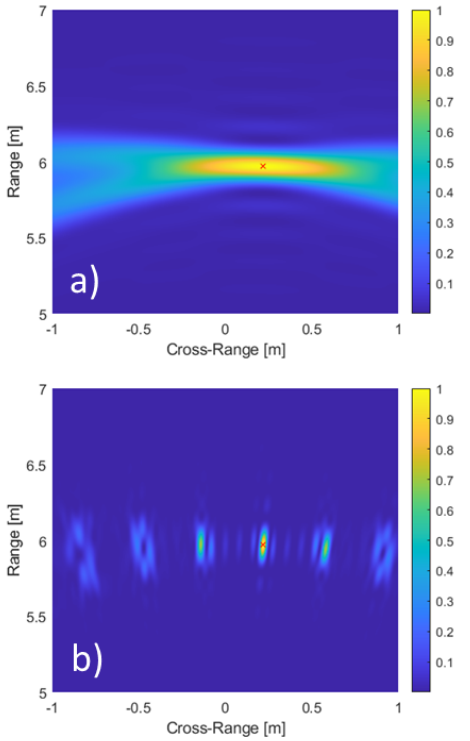

Fig. 5. Simulation results of the 2×4 VCSEL-based MIMO RaoF system: (a) non-coherent MIMO output, (b) coherent MIMO output.

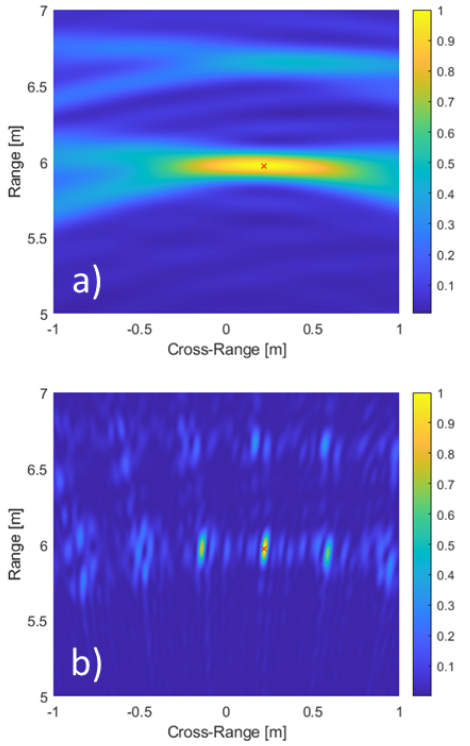

Fig. 6. Experimental results of the 2×4 VCSEL-based MIMO RaoF system: (a) non-coherent MIMO output, (b) coherent MIMO output.

propagation of the signal, which generates a ghost target. Unfortunately, in case of multipath propagation, the high range sidelobes propagating from the ghost target may interfere with the first target. This may produce an overall shift of the target-originated ellipsoid and worsen the final localization accuracy.

In case of coherent MIMO processing, in Fig. 6(b) it is possible to observe the same pattern observed in Fig. 5(b), along with the presence of much more secondary lobes appearing not only at the range of the true target, but also at the range of the ghost target. In theory, this problem should be somehow mitigated by the application of MIMO-ABF techniques.

B. MIMO Adaptive Beamforming

The results of the application of the MIMO-ABF techniques presented in Section III are reported in Fig. 7. In particular, the LS estimator output is shown in Fig. 7(a), the Capon beamformer in Fig. 7(b), and the RCB estimator in Fig. 7(c). In all the cases it is possible to observe a visible improvement in terms of the average sidelobe suppression capability of the system with respect to the result observed in Fig. 6(b).

However, the main sidelobe pattern is still evident as the one depicted in Fig. 5(b). This pattern is now visible for both the true and the ghost targets. In addition, all the three estimators provide very similar results and significant differences among them cannot be qualitatively appreciated.

Possible reasons for such results could lie in the fact that *i)* the considered experimental setup lays at the limit of validity of the far field assumption, *ii)* the target is not truly a point-like scatterer, and *iii)* a robust system calibration procedure needs to be developed.

TABLE I
ANALYSIS OF KEY PERFORMANCE INDICATORS

	dR [m]	**dXR** [m]	**PMSR** [dB]	**PASR** [dB]	**RMSE** [m]
MIMO	0.1580	0.0380	0.9536	13.6775	0.0292
LS	0.1525	0.0205	0.8372	15.8604	0.0296
Capon	0.1530	0.0245	0.9553	16.4706	0.0285
RCB	0.1520	0.0250	0.7483	16.6835	0.0287

C. Analysis of Key Performance Indicators

Following the procedure described in [26], key performance indicators (KPIs) are considered for evaluating average performance trends. In particular, range (dR) and cross-range (dXR) resolutions, root mean square error (RMSE) of the estimated target position, peak-to-maximum sidelobe ratio (PMSR) and peak-to-average sidelobe ratio (PASR) have been identified.

Results summarized in Table I have been averaged over 10 acquisitions, with the target at ≈ 6 m range placed at different cross-ranges. Although the limited sample space, it is possible to observe that MIMO-ABF techniques. compared with standard coherent MIMO processing, bring an improvement of about $1.5 \div 2$ times in terms of cross-range resolution, and apparently none in terms of range resolution. In terms of PMSR, no significant differences can be observed, except a small degradation (i.e., 0.2 dB). However, in terms of PASR, the improvement brought by MIMO-ABF techniques is about 3 dB. This result confirms the qualitative analysis presented

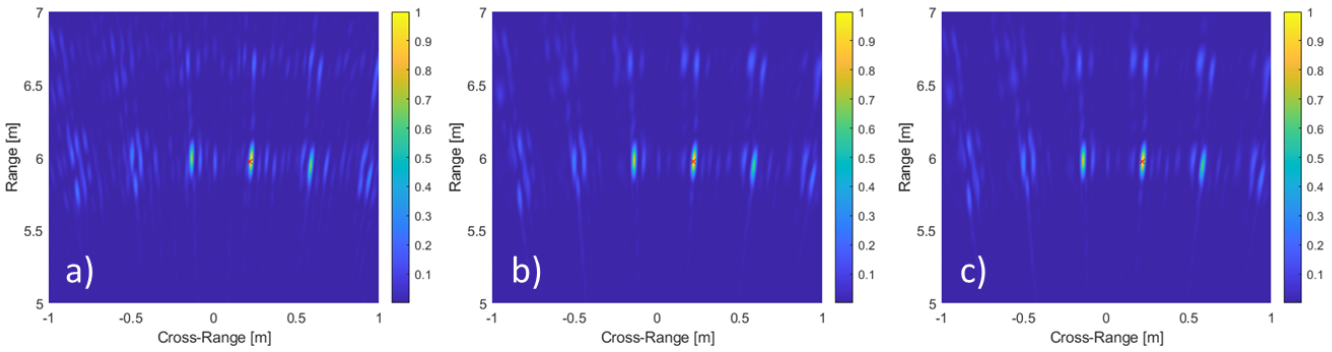

Fig. 7. Analysis of the adaptive beamforming algorithms for the 2×4 VCSEL-based MIMO RaoF expermental system: (a) LS estimator, (b) Capon estimator, (c) Robust Capon Beamformer.

in Section V-B. Finally, no significant differences can be observed in terms of target localization accuracy (i.e., RMSE).

VI. Conclusion

In this paper, adaptive beamforming (ABF) techniques have been applied to a VCSEL-based coherent multiple-input multiple-output (MIMO) radar-over-fiber (RaoF) system. Both data-independent and data-dependent MIMO-ABF techniques have been implemented. In particular, the least squares (LS), the Capon and the robust Capon beamformer (RCB) estimators have been considered. The effectiveness of standard MIMO and MIMO-ABF processing techniques has been investigated on X-band data collected by a MIMO RaoF system in a controlled scenario.

First, the experimental study case has been simulated to validate the non-coherent and coherent outputs of the standard MIMO processing. This analysis has revealed the possible presence of multipath propagation, which could worsen the expected processing outcomes.

Second, the three MIMO-ABF techniques have been applied to the real data. In all three cases it was possible to observe an improvement of about 3 dB in terms of the average sidelobe suppression capability, as well as cross-range resolution of about $1.5 \div 2$ times, of the system with respect to the coherent MIMO processing output. However, the MIMO ambiguity function pattern, as in the ideal case, was still visible. In addition, differences among the three estimators have provided very similar results in the considered experimental setup. Not exhaustive yet, this analysis requires further investigations.

References

[1] M. S. Greco, *et al.*, "Advances in radar systems for modern civilian and commercial applications," *IEEE Sig. Proc. Mag.*, vol. 36, no. 4, pp. 13-15, Jul. 2019.

[2] M. S. Greco, *et al.*, "Advances in radar systems for modern civilian and commercial applications," *IEEE Sig. Proc. Mag.*, vol. 36, no. 5, pp. 16-18, Sep. 2019.

[3] J. J. Alter, *et al.*, "Ubiquitous radar: An implementation concept," *Proc. IEEE Radar Conf.*, pp. 65-70, 2004.

[4] V. S. Chernyak, Fundamentals of Multisite Radar Systems, Routledge, 1998.

[5] E. Fishler, *et al.*, "MIMO radar: An idea whose time has come," *IEEE Radar Conf.*, pp. 71–78, 2004.

[6] J. Li, P. Stoica, "MIMO Radar with Colocated Antennas," *IEEE Sig. Proc. Mag.*, vol. 24, no. 5, pp. 106-114, Sept. 2007.

[7] A. M. Haimovich, *et al.*, "MIMO Radar with Widely Separated Antennas," *IEEE Sig. Proc. Mag.*, vol. 25, no. 1, pp. 116-129, 2008.

[8] E. Fishler, *et al.*, "Spatial diversity in radars—Models and detection performance", *IEEE Trans. Signal Process.*, vol. 54, pp. 823-838, 2006.

[9] N. Lehmann, *et al.*, "MIMO-radar application to moving target detection in homogenous clutter", Adaptive Sensor Array Processing Workshop at MIT Lincoln Laboratory, 2006.

[10] N. H. Lehmann, *et al.*, "High resolution capabilities of MIMO radar", Proc. 40th Asilomar Conf. Signals Systems and Computers, 2006.

[11] J. Capmany, D. Novak, "Microwave photonics combines two worlds", *Nature Photonics*, vol. 1, pp. 319-330, 2007.

[12] J. McKinney, "Photonics illuminates the future of radar", *Nature*, vol. 507, pp. 310-312, 2014.

[13] A. Bogoni, P. Ghelfi and F. Laghezza, Photonics for Radar Networks and Electronic Warfare Systems, London:IET SciTech Pub., 2019.

[14] G. Serafino, *et al.*, "Microwave Photonics for Remote Sensing: From Basic Concepts to High-Level Functionalities", *IEEE J. of Light. Tech.*, vol. 38, no. 19, pp. 5339-5355, 2020.

[15] A. Malacarne, *et al.*, "Coherent Dual-Band Radar-Over-Fiber Network With VCSEL-Based Signal Distribution," *IEEE J. Light. Technol.*, vol. 38, no. 22, pp. 6257-6264, 2020.

[16] D. M. Kuchta, *et al.*, "A 71-Gb/s NRZ modulated 850-nm VCSEL-based optical link," *IEEE Phot. Tech. Lett.*, vol. 27, no. 6, pp. 577-580, Mar. 2015.

[17] L. Xu, *et al.*, "Target detection and parameter estimation for MIMO radar systems," *IEEE Trans. Aerosp. Electron. Syst.*, vol. 44, no. 3, pp. 927-939, 2008.

[18] S. Maresca, *et al.*, "Analysis of Adaptive Beamforming Techniques for Photonics-based Coherent MIMO Radars," *2023 IEEE Int. Work. on Tech. for Def. and Sec. (TechDefense)*, Nov. 20-22, 2023, Rome, Italy.

[19] J. Capon, "High resolution frequency-wavenumber spectrum analysis," *Proc. IEEE*, vol. 57, pp. 1408—1418, 1969.

[20] J. Li, and P. Stoica, "An adaptive filtering approach to spectral estimation and SAR imaging", *IEEE Transactions on Signal Processing*, vol. 44, pp. 1469-1484, June 1996.

[21] A. Jakobsson, and P. Stoica, "Combining Capon and APES for estimation of spectral lines", *Circuits Systems and Signal Processing*, vol. 19, no. 2, pp. 159-169, 2000.

[22] L. Xu, P. Stoica and J. Li, "A diagonal growth curve model and some signal processing applications", *IEEE Trans. on Sig. Proc.*, vol. 54, pp. 3363-3371, Sept. 2006.

[23] J. Li, *et al.*, "On robust Capon beamforming and diagonal loading," *IEEE Trans. Signal Process.*, vol. 51, pp. 1702—1715, 2003.

[24] P. Stoica, Z. Wang, and J. Li, "Robust Capon beamforming", *IEEE Signal Processing Letters*, vol. 10, pp. 172-175, June 2003.

[25] J. Li, P. Stoica, and Z. Wang, "Doubly constrained robust Capon beamformer", *IEEE Transactions on Signal Processing*, vol. 52, pp. 2407-2423, Sept. 2004.

[26] G. Serafino, *et al.*, "Key Performance Indicators for System Analysis of MIMO Radars with Widely Separated Antennas," 19th European Radar Conference (EuRAD), Milan, Italy, 2022.